ARTICLE

Label-Free Optical Detection of Biomolecular Translocation through Nanopore Arrays

Andrey Ivankin,[†,⊥] Robert Y. Henley,[†,⊥] Joseph Larkin,[†] Spencer Carson,[†] Michael L. Toscano,[†] and Meni Wanunu[*,†,#]

[†]Department of Physics, Northeastern University, Boston, Massachusetts 02115, United States and [#]Department of Chemistry and Chemical Biology, Northeastern University, Boston, Massachusetts 02115, United States. [⊥]Andrey Ivankin and Robert Y. Henley contributed equally to this manuscript.

ABSTRACT In recent years, nanopores have emerged as exceptionally promising single-molecule sensors due to their ability to detect biomolecules at subfemtomole levels in a label-free manner. Development of a high-throughput nanopore-based biosensor requires multiplexing of nanopore measurements. Electrical detection, however, poses a challenge, as each nanopore circuit must be electrically independent, which requires complex nanofluidics and embedded electrodes. Here, we present an optical method for simultaneous measurements of the ionic current across an array of solid-state nanopores, requiring no additional fabrication steps. Proof-of-principle experiments are conducted that show simultaneous optical detection and characterization of ssDNA and dsDNA using an array of pores. Through a comparison with electrical measurements, we show that optical measurements are capable of accessing equivalent transmembrane current information.

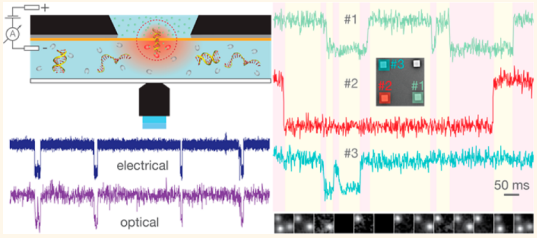

KEYWORDS: nanopore · ionophore · fluorescence · single-molecule · optical patch-clamping

Nanopores offer a unique capability of sensing and manipulating single molecules in a label-free manner. In a typical nanopore measurement, an insulating membrane separates two chambers containing an electrolyte solution; analyte molecules in the solution are electrophoretically driven across the barrier *via* a nanometer-scale aperture contained in the membrane. A characteristic transient drop in the ionic conductance of the pore is observed for each passing molecule, which is used to determine its identity. Over the past decade, nanopore-based techniques have shown great promise in a wide range of biophysical and biomedical applications, including DNA,[1,2] RNA,[3] and protein sequencing;[4−6] drug discovery;[7] single-molecule biophysics;[8,9] and proteomics.[10−13]

Due to the stochastic nature of single-molecule detection using nanopores, many discrete molecular observations are required in order to obtain statistically significant data for a sample. Multiplexed detection from an array of sensors can considerably speed up measurements, thereby reducing the molecular/biological sample requirement. Furthermore, the ability to introduce sensors tailored for different molecules on a single device can afford complex mixture analysis at unprecedentedly small volumes. However, a critical requirement for this is that each pore in the sensor array is monitored independently, which in the case of electrical detection requires advanced microfluidics and integrated circuitry. Indeed, various schemes have been proposed and demonstrated for multiplexed detection, which include optical approaches,[14−19] field effect/tunneling-based detection,[20−26] and fluid wells connected to electrode arrays.[27−29] Nonoptical approaches to reading multiple pores, namely, tunneling-based or fluid wells, are both limited by the need for a network of parallel electrodes and/or fluid conduits that lead to macroscale contacts. On-board amplifiers can alleviate the space requirements of integration, although a recent review estimated that a cost-effective integration would be limited to 1000 amplifiers in a 600 mm^2 chip area.[30] For comparison, in the Ion Torrent device, a similar sized chip can accommodate a million measurement

* Address correspondence to wanunu@neu.edu.

Received for review August 14, 2014 and accepted September 18, 2014.

Published online September 18, 2014
10.1021/nn504551d

chambers,[31] three orders-of-magnitude higher than on-board amplified nanopore circuits. Moreover, such nanopore array systems are comprised of two array chips that require alignment, one for circuitry and another for fluidics. Therefore, despite recent demonstrations of devices with arrays of 16 α-hemolysin nanopores,[27] 16 glass nanopore channels,[28] and an 8-channel α-hemolysin platform,[29] scaling up of the nanosensor and its readout is more space-consuming than the sensor itself.

In contrast, optical methods for multiplexed detection have made it possible to simultaneously observe optical signals in nanopores using labeled molecules.[14−19] However, the need for labeling the sample is restrictive, and detection is plagued with false negatives due to sample bleaching and imperfect labeling. Recently, a method was developed for monitoring ion flow through individual protein channels.[32−34] In this method, Ca^{2+} sensitive fluorescent dyes are used to monitor changes in Ca^{2+} concentration in the immediate vicinity of membrane channels. On the basis of this method, theoretical studies on ion channels have suggested that Ca^{2+}-based approaches can yield signal-to-noise ratios >10:1 at a millisecond time resolution.[35] Parallel optical readout of multipore ionic currents at these time resolutions is attractive for emerging nanopore applications, particularly for enzyme-driven DNA sequencing applications.[36−39] For these reasons, this approach has been adopted within the ion channel community for localizing and imaging the ionic current through multiple channels simultaneously.[40] Although this appears to be a viable strategy for parallelization of nanopore measurements, the only attempt, to our knowledge, to utilize the fluorescent sensing of ionic current through nanopores was made by Heron and co-workers.[41] However, this study provided only limited insight into the feasibility of the optical detection of ionic current in nanopore experiments, as no biomolecular translocation data was reported, optical imaging was performed at only 100 fps, and the high Ca^{2+} concentrations used were incompatible with most enzymatic applications. Finally, the approach was limited to lipid-embedded protein channels in a total-internal reflection fluorescence (TIRF) mode, which sets restrictions on the pore size range and the geometry of the setup.

Here we present the first example of Ca^{2+}-based epifluorescence detection of unlabeled DNA molecules passing through an array of solid-state nanopores. Using a flow channel underneath the membrane, we flow Ca^{2+} dye solution and detect ion currents through pores as small as 1.8 nm in diameter at millisecond time-resolutions. We demonstrate that the spacing between adjacent pores can be as small as a few micrometers, yielding the pore density on a chip comparable to that of Ion Torrent's device and at least

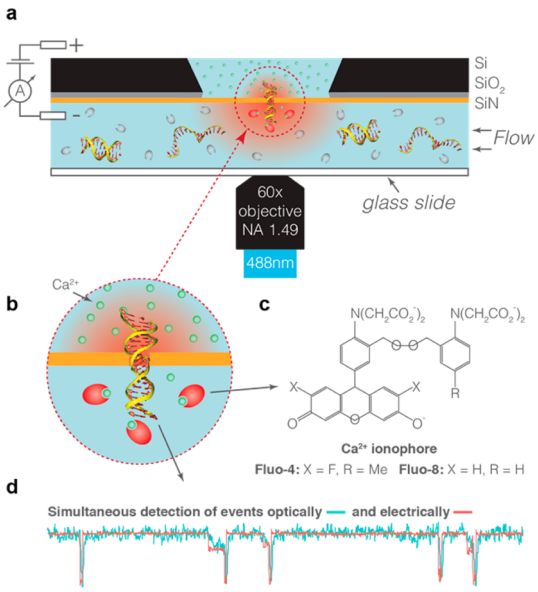

Figure 1. Simultaneous electrical and optical readout of ionic current in nanopores. (a) Schematic of the measurement setup. Both chambers of the experimental cell are equipped with Ag/AgCl electrodes for the electrical recording of the ionic current through the pore. (b) Zoomed-in view of the nanopore area. The optical detection of the ionic current is achieved by adding Ca^{2+} ions to the top (*trans*) chamber and Ca^{2+} ionophore to the bottom (*cis*) chamber of the cell. (c) Chemical structure of the ionophore. A voltage across the membrane drives Ca^{2+} ions to the *cis* side where they complex with the ionophore, resulting in fluorescence signal. The fluorescence intensity is proportional to the Ca^{2+} concentration and, thus, the flow of ions through the pore. Subsequently, a drop in the ionic current during a translocation event can be simultaneously detected from the decrease in the fluorescence intensity (d).

100× higher than any existing nanopore array device. Notably, we have performed these experiments at Ca^{2+} concentrations in which many biological motors, such as the DNA polymerase ϕ29 often utilized in sequencing applications, remain active (see SI). The ionic current information accessed by optical methods is equivalent to that found electrically, and therefore, our method paves the way for large-scale parallelization of a wide range of nanopore measurements.

RESULTS AND DISCUSSION

Our system is composed of one or more nanopores formed in a thin insulating silicon nitride membrane, suspended on a silicon chip frame (Figure 1a, Materials and Methods). The chip is mounted in a custom fluidic cell that permits simultaneous electrical and optical measurements of ionic current through a nanopore. The cell is equipped with channels for embedding Ag/AgCl electrodes on either side of the chip and exchanging buffer on the analyte *cis* side. To gain optical access to the membrane, the *cis* side of the chip is covered with a glass coverslip and then the cell is mounted on an inverted microscope with an oil immersion high NA objective (Nikon 60×/1.49). The *cis* chamber is filled with a solution of 0.4 M KCl, 1 mM

EDTA, 65 μM EGTA, 10 mM Tris buffered to pH 7.9, and 6.5 μM of Ca^{2+}-sensitive fluorescent dye Fluo-8 (unless otherwise noted) (Figure 1c). The opposite *trans* chamber of the cell is filled with a buffer containing 0.4 M KCl, 65 mM $CaCl_2$, and 10 mM Tris buffered to pH 7.9.

This system allows us to apply an electric field across the membrane and electrophoretically drive charged molecules across the pore. The cumulative flow across all pores in the system is monitored electrically by sampling the ionic current across the chip using an Axon Axopatch 200B patch-clamp amplifier. The distinctive feature of this system is the ability to optically monitor the flow of Ca^{2+} ions across each individual pore in parallel. As Ca^{2+} ions are driven across the pore, they form a complex with the calcium sensitive Fluo-8 fluorescent dye molecules. This fluorescent dye is excited by the 488 nm line of an argon-ion laser and exhibits an increase in fluorescent intensity of more than 100× upon binding to Ca^{2+}. The flow of Ca^{2+} ions can then be inferred by sampling the fluorescence levels at the site of each nanopore. To reduce background fluorescence, EGTA and EDTA agents were added to the *cis* chamber to chelate the remaining Ca^{2+} and Mg^{2+} ions.

The intensity of the localized fluorescent signal in the immediate vicinity of each pore is proportional to the Ca^{2+} flux through the pore and remains constant as long as the steady flow of ions and ionophores is maintained. A disruption of the ionic flow due to the presence of an analyte molecule in the pore results in an instantaneous reduction in fluorescence intensity. Thus, this technique optically accesses the same current information as patch-clamp experiments. This implies that all nanopore-based applications that rely on electrical ionic current measurements may be supplanted by optical current measurements. It is noteworthy that the optical readout of the ionic current possesses an advantage over the electrical measurements as it can be scaled up to multiple nanopores with ease. Moreover, in contrast to traditional fluorescent microscopy approaches, this approach is label-free.

Similar to other fluorescent reporter molecules, Fluo-8 is prone to photobleaching upon exposure to laser excitation. Figure 2a shows the exponential decay of the fluorescence intensity over time with a time constant $\tau \approx 1.6$ s, available from the fit. This implies that the fluorescent signal drops 5% over 80 ms or 50% in 1.1 s due to photobleaching. A brief calculation suggests that at these time scales diffusion alone is unable to warrant a supply of fresh dye molecules and prevent signal loss. We assume the diffusion constant (D) for the dye to be that of fluorescein, $D \approx 420$ nm$^2/\mu$s,[42] and that $2D$ diffusion away from the laser spot can be described by $\langle x^2 \rangle = 4Dt$, then the displacement $x =$ 20 μm in ~240 ms. The laser spot size used is of the order of 50 μm in diameter, which implies that with no flow a dye molecule is exposed to illumination for at

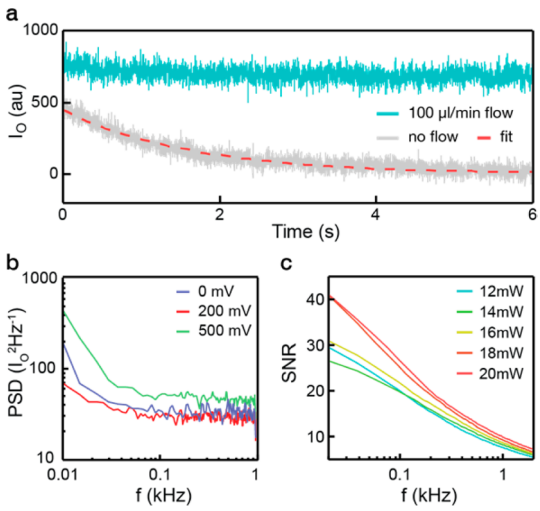

Figure 2. (a) The effect of flow on the intensity of the optical signal. When no flow is present, intensity decays exponentially due to photobleaching of the dye. (b) Power spectral density of the optical signal as a function of bandwidth for 0, 200, and 500 mV applied voltages across the membrane. (c) SNR as a function of bandwidth for the indicated laser powers.

least 600 ms. However, if we pump buffer through the *cis* chamber at a rate of 100 μL/min, dye molecules remain illuminated for as short as 12.5 ms, given the distance between the glass and the chip, 0.2 mm, and the channel width of 2 mm. Figure 2a demonstrates that such flow rate is sufficient to maintain the fluorescence intensity within 95% of its maximum for prolonged ion current measurements.

Nanopore noise power spectral density (PSD) for the optical signal readout at different voltages is presented in Figure 2b. At frequencies below 100 Hz, all traces display 1/*f*-type noise, followed with a relatively flat region up to 1 kHz. Because optical sensing assesses the same phenomenon as patch-clamp measurements, namely, transport of ions through a pore, we anticipate nanopore noise for both readouts to be of the same nature. The low 1/*f* flicker noise has been recently shown to arise from fluctuations in the number of charge carriers in a solid-state pore.[43] The Johnson noise arising from thermal fluctuations in the nanopore resistance dominates 1/*f* noise at higher frequencies (100 Hz to 1 kHz range). For 1 kHz sampling rate, the noise of the optical signal is negligibly affected by applying 200 mV bias; however, it increases 1.6 times when 500 mV is applied.

Although an increase in laser power can lead to the excitation of a larger volume of sample, and consequently higher optical signal, it may also result in higher noise, thus compromising the overall signal-to-noise ratio (SNR). We define SNR = $\langle I_O \rangle / I_{noise,RMS}$, where $\langle I_O \rangle$ is the mean of the optical signal and $I_{noise,RMS} = (\int_0^{BW} S_I \, df)^{1/2}$ is the root-mean-square current noise, where BW is the bandwidth. We find that SNR can be improved by raising the laser power, as shown

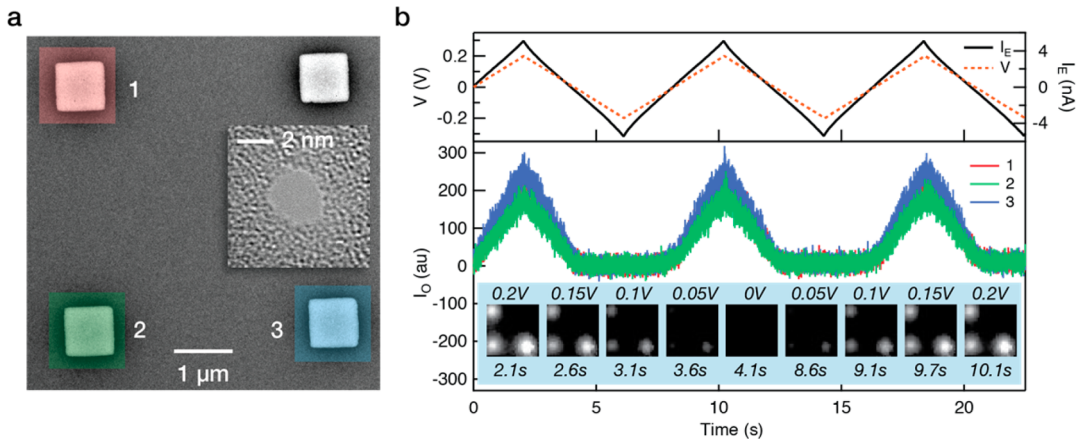

Figure 3. Simultaneous optical readout of ionic current through multiple nanopores. (a) Scanning electron microscopy (SEM) image of the chip with four locally thinned regions and with a 3 nm pore drilled in three of them (color-coded). The inset is a transmission electron microscopy (TEM) image of a typical pore. (b) Cumulative ionic current (I_E) and individual fluorescence intensity (I_O) responses from 3 pores to voltage in the ±0.2 V range (65 mM of $CaCl_2$ in *trans* and 6.5 μM of Fluo-4 in *cis* chamber). Bottom panel illustrates the evolution of fluorescence signal at the pores with voltage.

in Figure 2c; an increase in laser power from 12 to 20 mW leads to an improvement of SNR from 7.6 to 9.9. Furthermore, >7 independent measurements in various pores have showed a stable SNR value of 8.9 ± 2.2 (1 kHz sampling rate, 400 mV bias, 20 mW laser power). We anticipate that the use of high laser power densities can result in pore heating[44] and surface charge effects[45] that may negatively impact the SNR, although the data in Figure 2c indicates that we are well below this regime.

To assess the parallelization potential of optical readout as well as the correlation between electrical and optical signals, we studied optical signal response to changing voltage, an analogue of *I*−*V* curves. Arrays of 800 × 800 nm-thinned regions were patterned onto the membrane sides of our chips, to assist in optical localization of nanopores. In addition, it has been previously shown that the thinning of membranes can increase signal amplitude for biomolecule detection.[46] Figure 3a displays an SEM image of a typical nanopore array used in these experiments. Three nanopores with similar ∼3 nm diameters were drilled in the thinned regions indicated in the figure. The inset of Figure 3a shows a transmission electron microscopy image of a typical 3 nm diameter pore.

Figure 3b shows an example of simultaneous optical and electrical measurements of ionic flow through 3 nanopores as the voltage is repeatedly swept from −200 to +200 mV. The figure clearly shows that when a positive bias is applied a proportional increase in fluorescence can be observed at the location of any open pores, while a negative bias yields no increase in intensity as expected. The bottom panel of Figure 3b shows that no crosstalk is observed for an array of ∼3 nm diameter nanopores with ∼4 μm spacing, and it is important to note that the spacing can be further reduced as the nanopore diameter is reduced. In all experiments, the ionic current varies linearly with voltage, and similarly it can be seen that the fluorescent intensity from each pore varies linearly with voltage. Linear fits to the data yield the value of nanopore resistance. The resistance obtained from these measurements is 39.6 MΩ across all three pores.

To demonstrate the single molecule sensing ability of this system, a chip containing a single nanopore, ∼2.7 nm in diameter and ∼2 nm in effective thickness, was assembled as previously described, and a 1 nM concentration of 1000 bp dsDNA was added to the *cis* chamber buffer. Buffer was pumped through the *cis* chamber at a steady rate of 100 μL/min to minimize signal loss due to photobleaching. Figure 4a shows the resulting optical and electrical traces, with fluorescent intensity on the left axis and the ionic current on the right axis. For these traces a +200 mV bias was applied, optical data was collected at 4.8 kHz and downsampled to 1 kHz, while electrical data was collected at 20 kHz and low pass filtered to 10 kHz.

The presence of a translocating analyte molecule within the pore causes characteristic transient drops in both optical intensity and ionic current. The changes in ionic current (ΔI) and fluorescent intensity (ΔI_0) are proportional to the number of ions the molecule excludes from the pore. The duration of the event, or dwell time (t_d), is defined by the amount of time the molecule resides in the pore. Both traces were analyzed and the dwell time measurements for each translocation event were extracted. Corresponding current drop values were extracted from electrical traces, and corresponding optical intensity drops were extracted from optical traces. Analysis was performed using the open source data analysis software OpenNanopore from the Radenovic lab at EPFL.[47] Examples of analyzed optical and electrical events are shown in Figure 4b and longer traces of concatenated analyzed events can be found in Supporting Information,

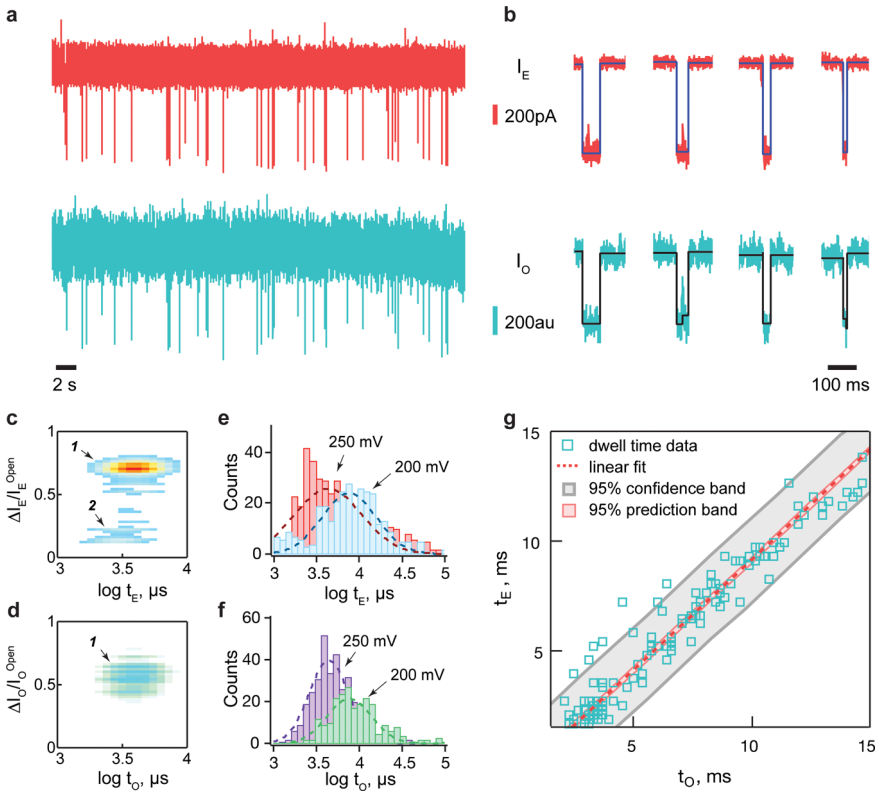

Figure 4. Optical *vs* electrical dsDNA translocation detection. (a) Continuous optical and electrical traces of events for 1000 bp dsDNA at 200 mV (65 mM of $CaCl_2$ in *trans* and 6.5 μM of Fluo-8 in *cis* chamber) and examples of event fits are shown in (b). Optical data is collected at 4.8 kHz and down-sampled to 1 kHz and electrical data is collected at 20 kHz and low pass filtered to 10 kHz. Contour plots of events from a subset of the 200 mV data detected (c) electrically and (d) optically (population 1 represents DNA translocation events and population 2 are DNA collisions). Both contour plots display data from 226 events. Histograms of (e) electrically and (f) optically detected events at applied potentials of 200 and 250 mV. (g) Correlation between dsDNA translocation times detected electrically t_E and optically t_O in the range 1.5–15 ms (blue open circles represent experimental data and red dashed line is a fit with a slope of 1.001 ± 0.001 and an intercept of 0 ms). The data here consists of 294 events collected over the course of 3 different experiments with 3 different pores that varied in size from 2.5 to 3.0 nm. Note that the 95% prediction band overlaps with the curve fit (dashed red line).

Figure S1. Figures 4c shows a contour plot for the translocation events detected electrically and Figure 4d shows the corresponding data from optical measurements. A comparison of the two contour plots shows good agreement between dwell times for the translocation populations. Figure 4e shows histograms for the log of the dwell time values observed in electrical measurements; data is presented for applied biases of 250 and 200 mV. Corresponding optical histograms are displayed in Figure 4f. Gaussian fits to these histograms are displayed to estimate the peaks of the distributions. For 200 mV, electrical measurements indicate a most likely dwell time of 7.6 ms, while optical measurements suggest this value is 7.5 ms. For an applied voltage of 250 mV, the most likely dwell time observed electrically is 4.3 ms, whereas optically this value is 4.4 ms.

To further quantify the correlation between the two signals, we plotted observed electrical dwell time values against optical dwell time values for 294 events over 3 different single pore experiments (Figure 4g). A perfect correlation between these two signals would result in the data forming a straight line with a slope of 1. A least-squares regression analysis of the data produced a line with a slope of 1.001 ± 0.001. These results show a strong correlation between optical and electrical measurements, once again implying that optical measurements are able to access the same information as conventional nanopore experiments.

Electrical measurements suggest the presence of two distinctive populations of events (Figure 4c). On the basis of the ionic current blockades $\Delta I_E/I_E^{Open}$ of 0.72 ± 0.06 (1) and 0.18 ± 0.09 (2) (see histogram fits in Supporting Information Figure S2), we assign population 1 to DNA translocation events, whereas population 2 presumably corresponds to collisions. Interestingly, the collision population 2 is completely missing in the optical scatter plot (Figure 4d). Moreover, according to the optical measurements, DNA molecules block a smaller fraction of the ionic current with $\Delta I_O/I_O^{Open}$ comprising 0.56 ± 0.15. Since the optical readout is selective to Ca^{2+} ions, both of these discrepancies may be related to the difference in how Ca^{2+} and monovalent ions interact with DNA.[48]

Notably, optical measurements maintain a high signal-to-noise ratio during DNA translocation; this ratio can be defined as $SNR_{DNA} = \Delta I_O/I_{noise,RMS}$,

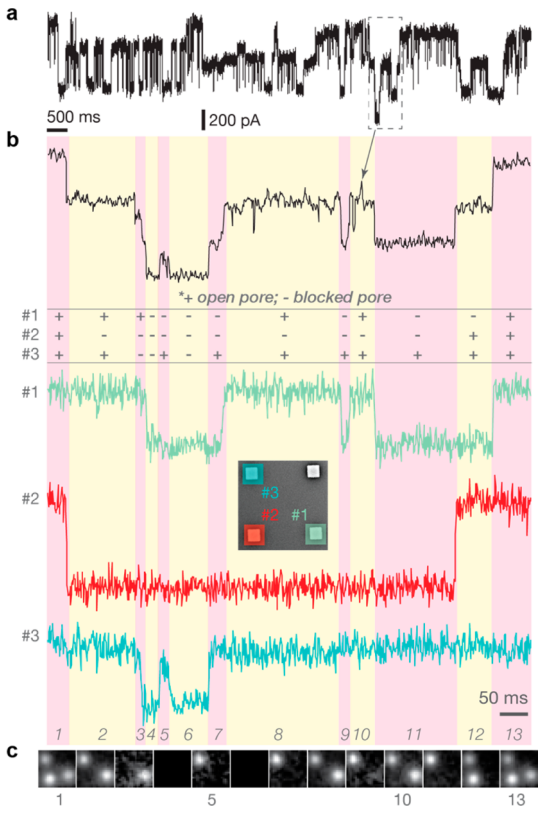

Figure 5. Simultaneous detection of ssDNA translocation events through multiple pores. (a) Cumulative electrical trace of 153 nt-long ssDNA translocation events thru 3 sub-2 nm pores at the applied potential of 400 mV. (b) Zoomed-in region of the electrical trace with a multilevel event accompanied by the optical traces for each pore (65 mM of $CaCl_2$ in *trans* and 6.5 μM of Fluo-8 in *cis* chamber). (c) Fluorescence intensity images of the pores averaged over the corresponding frames.

where ΔI_O is the drop in the optical intensity upon translocation of DNA. For 5 independent measurements, $SNR_{DNA} = 7 \pm 1.5$ for a bias of 400 mV and 1 kHz sampling rate.

To display the scalability of this technique, an array of 3 sub-2 nm pores was drilled in a silicon nitride membrane and the system was assembled as before. For this experiment, 153 nt ssDNA was added to the previously described *cis* chamber buffer for a final concentration of 8 nM. A voltage bias of 400 mV was applied across the membrane, electrophoretically driving DNA molecules across all open pores. A representative electrical current trace can be seen in Figure 5a. The multiple distinct levels that can be observed correspond to analyte molecules translocating through different combinations of the three open pores. However, electrical measurements only describe the collective behavior of the system and are unable to provide the information about individual pores. In contrast, optical readout of the ionic current allows us to trace every change in the electrical current to a specific pore (Figure 5b). Figure 5c shows the optical signals from the pores over the course of 13 changes in the electrical current trace. A movie of the optical signal is included as Supporting Information.

CONCLUSION

In conclusion, we have demonstrated a method for parallelized solid-state nanopore ion current measurements that require no additional fabrication steps, embedded electrodes, or compartmentalized on-chip fluidics. To our knowledge, this is the first report of optical, label-free characterization of biomolecular translocation at millisecond time resolution using an array of synthetic nanopores. Our method uses fluorescence measurements to optically access the same information that can be attained through electrical current measurements. This technique may be of particular importance when low salt concentration is necessary, as all optical measurements here were performed with only 65 mM of $CaCl_2$. Notably, this concentration of calcium is compatible with the ϕ29 polymerase used in certain nanopore sequencing platforms[36,39] (see Supporting Information for details). If the desired system does not require such proteins, the calcium concentration used may be easily increased to attain a higher signal-to-noise ratio. This system may also be useful for simultaneously characterizing translocation dynamics of an analyte molecule through various pore diameters, as pores of varying sizes can be easily incorporated into the platform. We note that our system used epi-fluorescence illumination and an electron-multiplying CCD (emCCD) for detection, both of which can be improved upon in a more dedicated system by choosing the appropriate conditions (*e.g.*, sheet illumination and APD array detection). Finally, under the appropriate illumination/detection conditions, scaling up to a large array of small pores (which can be slow using TEM-based fabrication)[49] should be possible using recently demonstrated pore arrays that were fabricated using a scanning ion beam.[50]

MATERIALS AND METHODS

Schematics of the nanopore fluidic cell and experimental setup are shown in Supporting Information Figure S4. Nanopores were fabricated in ultrathin silicon nitride membranes as described previously.[46] Briefly, a 500-μm-thick silicon wafer with ⟨100⟩ crystal orientation and 2.5 μm of thermal oxide was coated with 100 nm of low-stress chemical vapor deposition silicon nitride (SiN). Standard UV photolithography was used to pattern square openings on one side of the wafer, through which the nitride and oxide were etched using SF_6 plasma. The photoresist was stripped, and an anisotropic etch followed by removal of the oxide layer resulted in ~30 μm × 30 μm free-standing windows on the reverse side of the wafer.

A film of poly(methyl methacrylate) (PMMA) was spun onto the membrane side of the window, and electron-beam lithography was used to pattern an array of small square openings of 800 nm × 800 nm or smaller 1.5−3 μm apart. SF_6 plasma etch locally thinned the SiN in these regions to ∼20 nm to increase the signal while maintaining the membrane's mechanical integrity. The PMMA was removed by incubation in acetone. A single nanopore or an array of nanopores was drilled through the thinned regions (no more than a pore per thinned region) of the SiN membrane using a JEOL 2010F transmission electron microscope. Fabricated pores were 1.5−10 nm in diameter, depending on the application.

The nanopore chip was cleaned in piranha acid using a procedure described previously.[51] After rinsing and drying of the chip, it was immediately mounted onto a custom-designed PEEK fluidic cell using silicone elastomer. The cell contains PEEK screws that allow pressure connection to syringe pumps to enable buffer flow at controlled rates. The silicone was painted over and around the membrane-facing side of the chip leaving <4 mm^2 area around the membrane, and a piranha-cleaned, rinsed and dried #1 glass coverslip was pressed against the chip. Homemade Ag/AgCl electrodes were immersed in each chamber of the cell and connected to an Axon 200B headstage. All measurements were taken in a dark Faraday cage. Electrical and optical signals were acquired using custom LabVIEW software. The analog current signal from the amplifier was low-pass filtered at 10 kHz and fed to a DAQ card, which sampled the data at 100 kHz/16 bit.

For all experiments, unless otherwise specified, membranes were epi-illuminated by feeding a 20 mW, 488 nm laser power beam (Coherent Sapphire) to the back of an inverted microscope (Olympus IX71) and through an oil immersion high NA objective (Nikon 60×/1.49). High-bandwidth fluorescence detection was achieved using an emCCD camera (Andor, iXon Ultra 897) in crop mode, which allowed frame rates of 2000−4800 frames/s. Synchronization between the electrical and optical signals was achieved by connecting the camera TTL pulse to the main DAQ board (PCI-6630, National Instruments) used for the acquisition of the electrical signal. The fluorophore molecules in the *cis* chamber were continuously replenished by pumping at a flow rate of 100 μL/min.

Custom MATLAB code was used for background subtraction, image filtering, and extraction of fluorescent intensity. Current traces and optical intensity traces were analyzed using the OpenNanopore software[47] to obtain dwell time and current blockage of events.

Conflict of Interest: The authors declare no competing financial interest.

Supporting Information Available: Scheme of experimental setup, phi29 extension assay in Ca^{2+}, optical data, and movie of array from Figure 5 (avi file). This material is available free of charge *via* the Internet at http://pubs.acs.org.

Acknowledgment. We gratefully acknowledge Martin Langecker for assistance with the LabVIEW interface to the measurement hardware. This work was supported by funding from the National Institutes of Health (R21-HG006873; R01-HG006321). This work was performed in part at the Cornell NanoScale Facility, a member of the National Nanotechnology Infrastructure Network, which is supported by the National Science Foundation (Grant ECCS-0335765).

REFERENCES AND NOTES

1. Branton, D.; Deamer, D. W.; Marziali, A.; Bayley, H.; Benner, S. A.; Butler, T.; Di Ventra, M.; Garaj, S.; Hibbs, A.; Huang, X.; *et al.* The Potential and Challenges of Nanopore Sequencing. *Nat. Biotechnol.* **2008**, *26*, 1146–1153.
2. Clarke, J.; Wu, H.-C.; Jayasinghe, L.; Patel, A.; Reid, S.; Bayley, H. Continuous Base Identification for Single-Molecule Nanopore DNA Sequencing. *Nat. Nanotechnol.* **2009**, *4*, 265–270.
3. Ayub, M.; Hardwick, S. W.; Luisi, B. F.; Bayley, H. Nanopore-Based Identification of Individual Nucleotides for Direct RNA Sequencing. *Nano Lett.* **2013**, *13*, 6144–6150.
4. Nivala, J.; Marks, D. B.; Akeson, M. Unfoldase-Mediated Protein Translocation through an Alpha-Hemolysin Nanopore. *Nat. Biotechnol.* **2013**, *31*, 247–250.
5. Rodriguez-Larrea, D.; Bayley, H. Multistep Protein Unfolding During Nanopore Translocation. *Nat. Nanotechnol.* **2013**, *8*, 288–295.
6. Rosen, C. B.; Rodriguez-Larrea, D.; Bayley, H. Single-Molecule Site-Specific Detection of Protein Phosphorylation with a Nanopore. *Nat. Biotechnol.* **2014**, *32*, 179–181.
7. Shasha, C.; Henley, R. Y.; Stoloff, D. H.; Rynearson, K. D.; Hermann, T.; Wanunu, M. Nanopore-Based Conformational Analysis of a Viral RNA Drug Target. *ACS Nano* **2014**, *8*, 6425–6430.
8. Arnaut, V.; Langecker, M.; Simmel, F. C. Nanopore Force Spectroscopy of Aptamer-Ligand Complexes. *Biophys. J.* **2013**, *105*, 1199–1207.
9. Keyser, U. F.; Koeleman, B. N.; Van Dorp, S.; Krapf, D.; Smeets, R. M. M.; Lemay, S. G.; Dekker, N. H.; Dekker, C. Direct Force Measurements on DNA in a Solid-State Nanopore. *Nat. Phys.* **2006**, *2*, 473–477.
10. Freedman, K. J.; Bastian, A. R.; Chaiken, I.; Kim, M. J. Solid-State Nanopore Detection of Protein Complexes: Applications in Healthcare and Protein Kinetics. *Small* **2013**, *9*, 750–759.
11. Japrung, D.; Dogan, J.; Freedman, K.; Nadzeyka, A.; Bauerdick, S.; Albrecht, T.; Kim, M. J.; Jemth, P.; Edel, J. B. Single-Molecule Studies of Intrinsically Disordered Proteins Using Solid-State Nanopores. *Anal. Chem.* **2013**, *85*, 2449–2456.
12. Larkin, J.; Henley, R. Y.; Muthukumar, M.; Rosenstein, J. K.; Wanunu, M. High-Bandwidth Protein Analysis Using Solid-State Nanopores. *Biophys. J.* **2014**, *106*, 696–704.
13. Li, W.; Bell, N. A. W.; Hernandez-Ainsa, S.; Thacker, V. V.; Thackray, A. M.; Bujdoso, R.; Keyser, U. F. Single Protein Molecule Detection by Glass Nanopores. *ACS Nano* **2013**, *7*, 4129–4134.
14. Chansin, G. A. T.; Mulero, R.; Hong, J.; Kim, M. J.; Demello, A. J.; Edel, J. B. Single-Molecule Spectroscopy Using Nanoporous Membranes. *Nano Lett.* **2007**, *7*, 2901–2906.
15. Soni, G. V.; Singer, A.; Yu, Z. L.; Sun, Y. J.; McNally, B.; Meller, A. Synchronous Optical and Electrical Detection of Biomolecules Traversing through Solid-State Nanopores. *Rev. Sci. Instrum.* **2010**, *81*, 014301.
16. McNally, B.; Singer, A.; Yu, Z. L.; Sun, Y. J.; Weng, Z. P.; Meller, A. Optical Recognition of Converted DNA Nucleotides for Single-Molecule DNA Sequencing Using Nanopore Arrays. *Nano Lett.* **2010**, *10*, 2237–2244.
17. Ando, G.; Hyun, C.; Li, J. L.; Mitsui, T. Directly Observing the Motion of DNA Molecules near Solid-State Nanopores. *ACS Nano* **2012**, *6*, 10090–10097.
18. Kurz, V.; Nelson, E. M.; Shim, J.; Timp, G. Direct Visualization of Single-Molecule Translocations through Synthetic Nanopores Comparable in Size to a Molecule. *ACS Nano* **2013**, *7*, 4057–4069.
19. Auger, T.; Mathe, J.; Viasnoff, V.; Charron, G.; Di Meglio, J. M.; Auvray, L.; Montel, F. Zero-Mode Waveguide Detection of Flow-Driven DNA Translocation through Nanopores. *Phys. Rev. Lett.* **2014**, *113*, 028302.
20. Ivanov, A. P.; Instuli, E.; McGilvery, C. M.; Baldwin, G.; McComb, D. W.; Albrecht, T.; Edel, J. B. DNA Tunneling Detector Embedded in a Nanopore. *Nano Lett.* **2011**, *11*, 279–285.
21. Tsutsui, M.; Matsubara, K.; Ohshiro, T.; Furuhashi, M.; Taniguchi, M.; Kawai, T. Electrical Detection of Single Methylcytosines in a DNA Oligomer. *J. Am. Chem. Soc.* **2011**, *133*, 9124–9128.
22. Healy, K.; Ray, V.; Willis, L. J.; Peterman, N.; Bartel, J.; Drndic, M. Fabrication and Characterization of Nanopores with Insulated Transverse Nanoelectrodes for DNA Sensing in Salt Solution. *Electrophoresis* **2012**, *33*, 3488–3496.
23. Xie, P.; Xiong, Q. H.; Fang, Y.; Qing, Q.; Lieber, C. M. Local Electrical Potential Detection of DNA by Nanowire-Nanopore Sensors. *Nat. Nano* **2012**, *7*, 119–125.
24. Krishnakumar, P.; Gyarfas, B.; Song, W. S.; Sen, S.; Zhang, P. M.; Krstic, P.; Lindsay, S. Slowing DNA Trans Location through a Nanopore Using a Functionalized Electrode. *ACS Nano* **2013**, *7*, 10319–10326.

25. Traversi, F.; Raillon, C.; Benameur, S. M.; Liu, K.; Khlybov, S.; Tosun, M.; Krasnozhon, D.; Kis, A.; Radenovic, A. Detecting the Translocation of DNA through a Nanopore Using Graphene Nanoribbons. *Nat. Nano* **2013**, *8*, 939–945.
26. Zhao, Y. A.; Ashcroft, B.; Zhang, P. M.; Liu, H.; Sen, S. M.; Song, W.; Im, J.; Gyarfas, B.; Manna, S.; Biswas, S.; *et al.* Single-Molecule Spectroscopy of Amino Acids and Peptides by Recognition Tunnelling. *Nat. Nanotechnol.* **2014**, *9*, 466–473.
27. Baaken, G.; Ankri, N.; Schuler, A.-K.; Ruehe, J.; Behrends, J. C. Nanopore-Based Single-Molecule Mass Spectrometry on a Lipid Membrane Microarray. *ACS Nano* **2011**, *5*, 8080–8088.
28. Bell, N. A. W.; Thacker, V. V.; Hernandez-Ainsa, S.; Fuentes-Perez, M. E.; Moreno-Herrero, F.; Liedl, T.; Keyser, U. F. Multiplexed Ionic Current Sensing with Glass Nanopores. *Lab Chip* **2013**, *13*, 1859–1862.
29. Osaki, T.; Suzuki, H.; Le Pioufle, B.; Takeuchi, S. Multichannel Simultaneous Measurements of Single-Molecule Translocation in Alpha-Hemolysin Nanopore Array. *Anal. Chem.* **2009**, *81*, 9866–9870.
30. Maitra, R. D.; Kim, J.; Dunbar, W. B. Recent Advances in Nanopore Sequencing. *Electrophoresis* **2012**, *33*, 3418–3428.
31. Rothberg, J. M.; Hinz, W.; Rearick, T. M.; Schultz, J.; Mileski, W.; Davey, M.; Leamon, J. H.; Johnson, K.; Milgrew, M. J.; Edwards, M.; *et al.* An Integrated Semiconductor Device Enabling Non-Optical Genome Sequencing. *Nature* **2011**, *475*, 348–352.
32. Demuro, A.; Parker, I. Optical Single-Channel Recording: Imaging Ca^{2+} Flux through Individual N-Type Voltage-Gated Channels Expressed in Xenopus Oocytes. *Cell Calcium* **2003**, *34*, 499–509.
33. Demuro, A.; Parker, I. Imaging the Activity and Localization of Single Voltage-Gated Ca^{2+} Channels by Total Internal Reflection Fluorescence Microscopy. *Biophys. J.* **2004**, *86*, 3250–3259.
34. Demuro, A.; Parker, I. "Optical Patch-Clamping": Single-Channel Recording by Imaging Ca^{2+} Flux through Individual Muscle Acetylcholine Receptor Channels. *J. Gen Phys.* **2005**, *126*, 179–192.
35. Shuai, J. W.; Parker, I. Optical Single-Channel Recording by Imaging Ca^{2+} Flux through Individual Ion Channels: Theoretical Considerations and Limits to Resolution. *Cell Calcium* **2005**, *37*, 283–299.
36. Manrao, E. A.; Derrington, I. M.; Laszlo, A. H.; Langford, K. W.; Hopper, M. K.; Gillgren, N.; Pavlenok, M.; Niederweis, M.; Gundlach, J. H. Reading DNA at Single-Nucleotide Resolution with a Mutant Mspa Nanopore and Phi29 DNA Polymerase. *Nat. Biotechnol.* **2012**, *30*, 349–353.
37. Laszlo, A. H.; Derrington, I. M.; Brinkerhoff, H.; Langford, K. W.; Nova, I. C.; Samson, J. M.; Bartlett, J. J.; Pavlenok, M.; Gundlach, J. H. Detection and Mapping of 5-Methylcytosine and 5-Hydroxymethylcytosine with Nanopore Mspa. *Proc. Natl. Acad. Sci. U.S.A.* **2013**, *110*, 18904–18909.
38. Schreiber, J.; Wescoe, Z. L.; Abu-Shumays, R.; Vivian, J. T.; Baatar, B.; Karplus, K.; Akeson, M. Error Rates for Nanopore Discrimination among Cytosine, Methylcytosine, and Hydroxymethylcytosine Along Individual DNA Strands. *Proc. Natl. Acad. Sci. U.S.A.* **2013**, *110*, 18910–18915.
39. Cherf, G. M.; Lieberman, K. R.; Rashid, H.; Lam, C. E.; Karplus, K.; Akeson, M. Automated Forward and Reverse Ratcheting of DNA in a Nanopore at 5-Angstrom Precision. *Nat. Biotechnol.* **2012**, *30*, 344–348.
40. Sonnleitner, A.; Isacoff, E. Single Ion Channel Imaging. *Methods Enzymol.* **2003**, *361*, 304–319.
41. Heron, A. J.; Thompson, J. R.; Cronin, B.; Bayley, H.; Wallace, M. I. Simultaneous Measurement of Ionic Current and Fluorescence from Single Protein Pores. *J. Am. Chem. Soc.* **2009**, *131*, 1652–1653.
42. Lukacs, G. L.; Haggie, P.; Seksek, O.; Lechardeur, D.; Freedman, N.; Verkman, A. S. Size-Dependent DNA Mobility in Cytoplasm and Nucleus. *J. Biol. Chem.* **2000**, *275*, 1625–1629.
43. Smeets, R. M. M.; Keyser, U. F.; Dekker, N. H.; Dekker, C. Noise in Solid-State Nanopores. *Proc. Natl. Acad. Sci. U.S.A.* **2008**, *105*, 417–421.
44. Keyser, U. F.; Krapf, D.; Koeleman, B. N.; Smeets, R. M. M.; Dekker, N. H.; Dekker, C. Nanopore Tomography of a Laser Focus. *Nano Lett.* **2005**, *5*, 2253–2256.
45. Di Fiori, N.; Squires, A.; Bar, D.; Gilboa, T.; Moustakas, T. D.; Meller, A. Optoelectronic Control of Surface Charge and Translocation Dynamics in Solid-State Nanopores. *Nat. Nano* **2013**, *8*, 946–951.
46. Wanunu, M.; Dadosh, T.; Ray, V.; Jin, J.; McReynolds, L.; Drndic, M. Rapid Electronic Detection of Probe-Specific Micrornas Using Thin Nanopore Sensors. *Nat. Nanotechnol.* **2010**, *5*, 807–814.
47. Raillon, C.; Granjon, P.; Graf, M.; Steinbock, L. J.; Radenovic, A. Fast and Automatic Processing of Multi-Level Events in Nanopore Translocation Experiments. *Nanoscale* **2012**, *4*, 4916–4924.
48. Egli, M. DNA-Cation Interactions: Quo Vadis? *Chem. Biol.* **2002**, *9*, 277–286.
49. Kim, M. J.; Wanunu, M.; Bell, D. C.; Meller, A. Rapid Fabrication of Uniformly Sized Nanopores and Nanopore Arrays for Parallel DNA Analysis. *Adv. Mater.* **2006**, *18*, 3149–3155.
50. Sawafta, F.; Clancy, B.; Carlsen, A. T.; Huber, M.; Hall, A. R. Solid-State Nanopores and Nanopore Arrays Optimized for Optical Detection. *Nanoscale* **2014**, *6*, 6991–6996.
51. Wanunu, M.; Meller, A. Chemically Modified Solid-State Nanopores. *Nano Lett.* **2007**, *7*, 1580–1585.